Thick-target-method study of $M_{\alpha\beta}$ x-ray production cross sections of Pb and Bi impacted by positrons up to 9 keV

Y. Wu,[1,*] Y. Liang,[1] M. X. Xu,[1] Y. Yuan,[1] C. H. Chang,[1] Z. C. Qian,[1] B. Y. Wang,[2] P. Kuang,[2] and P. Zhang[2]

[1]*Beijing Key Laboratory of Passive Safety Technology for Nuclear Energy, School of Nuclear Science and Engineering, North China Electric Power University, Beijing 102206, China*
[2]*Institute of High Energy Physics, Chinese Academy of Sciences, Beijing 100049, China*

Atomic M-shell x-ray production cross sections induced by positrons near the threshold energy have been presented in this paper. In the experiment, online monitoring technology, which utilizes a high-purity germanium detector to record the annihilation photons emitted from the pure thick target impacted by positrons, was developed to obtain the accurate number of the incident positrons. The effects of the multiple scattering of incident positrons, from the bremsstrahlung and annihilation photons and other secondary particles on the experimental characteristic x-ray yield, were eliminated by Monte Carlo simulation in combination with theoretical integral calculation. The Tikhonov regularization method was adopted to handle the ill-posed inverse problem involved in the thick-target method, i.e., x-ray production cross sections by the corrected characteristic x-ray yield. Experimental results of $M_{\alpha\beta}$ x-ray production cross sections for Pb and Bi impacted by 6–9-keV positrons were compared with the corresponding values predicted by the distorted-wave Born approximation (DWBA). Good agreement was found between the two. Moreover, we have presented the experimental results on the ratios of the $M_{\alpha\beta}$ x-ray production cross sections by electron impact in the literature to that by 6–9-keV positron impact in this work. They were also in accordance with the theoretical ratios calculated by the predictions of DWBA theory.

I. INTRODUCTION

Atomic inner-shell ionization by lepton impact for energies ranging from the ionization threshold up to four times this value plays an important role in both fundamental studies and practical applications [1]. Although some theoretical models near the atomic ionization threshold energy such as the plane-wave Born approximation theory with Coulomb, exchange, and relativistic corrections (PWBA-C-Ex) [2–5] and the distorted-wave Born approximation theory (DWBA) [3,6] have been proposed, the validity of these theoretical models needs to be demonstrated by lots of experimental data. However, the experimental data of atomic inner-shell ionization cross sections are still limited. For ionization by electron impact within four times the ionization threshold energy, several experimental results [7–13] have been published in recent years, these results show that the DWBA theory could give a relatively good description of the ionization process for electron impact. While for positron impact, the experimental data are very scarce [14–17], which limits obtaining a more accurate assessment of theoretical models. The reason for the lack of experimental data about positron impact is that a positron beam is harder to obtain than an electron beam. Besides, for positron impact, great difficulties in experiment and data analysis techniques remain unsolved. Up to now, the experimental data for positron impact within four times the ionization threshold energy are restricted to the K shell

of low atomic number (Z) elements (Ti ($Z = 22$) [17], Cu ($Z = 29$) [14]) and the L shell of medium-Z elements (Ag ($Z = 47$) [14], In ($Z = 49$), and Sn ($Z = 50$) [15]), while the experimental data are not involved in the M shell or high-Z elements. In order to completely verify the validity of the theoretical models, we measured the $M_{\alpha\beta}$ x-ray production cross sections of Pb ($Z = 82$) and Bi ($Z = 83$) by 6–9-keV positron impact in this work. Because the intensity of a positron beam based on the positron sources was low (it is hard to reach 10^6 e^+/s), here we used the pure thick-target sample [if we used the thin-target sample, for the silicon drift detector (SDD) [18] adopted in our experiment, it would be very time consuming for collecting interesting characteristic x-ray counts which can meet statistical requirements]. The Tikhonov regularization method has been adopted to handle the inverse problem involved in the thick-target method by An *et al.* [19], but the published experimental data processed by the Tikhonov method were only for the K shell, regardless of electron impact (K_α of Ni [19], $K_{\alpha\beta}$ of Si [20]) or positron impact (K_α of Ti [17]). The L or M shell has more characteristic x-ray subpeaks than the K shell; if each of the experimental characteristic x-ray subpeaks of the L or M shell cannot be separated by an x-ray energy spectrometer, it will be difficult to apply the Tikhonov regularization method to figure out L- or M-shell x-ray production cross sections involved in the thick-target method. Here we overcame the problem.

This paper is organized as follows. In the next section, the experimental setup and data processing are introduced. The Results and Discussion are presented in Sec. III. Finally, conclusions are given.
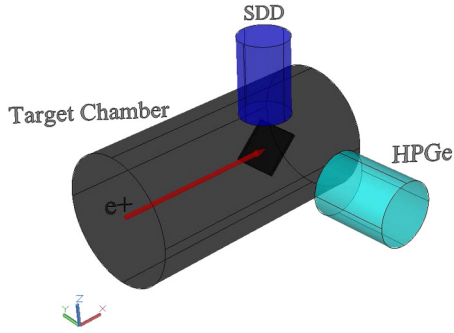
*Corresponding author: w_y@ncepu.edu.cn

FIG. 1. Diagram of experimental setup.

II. EXPERIMENT AND DATA PROCESSING

A. Experimental setup

Our experiment was performed at the newly introduced slow positron beam apparatus at the Key Laboratory of Nuclear Analysis Techniques at the Institute of High Energy Physics. Details of the newly introduced slow positron beam apparatus have been reported in Refs. [21,22]. The positrons were generated from a 50-mCi ^{22}Na [22] radioactive source, and moderated in a solid neon moderator, and then accelerated to the desired energies by the negative high voltage on the target holder. The intensity of the positron beam was $\sim 10^5$ e^+/s generally, the beam diameter at the target surface was about 3 mm, and the base pressure of the target chamber was $\sim 10^{-6}$ Pa. A diagram of the experimental setup is shown in Fig. 1. As can be seen, the positron beam was transported horizontally along the X axis into the chamber, and the thick target was placed with an angle of 45° to the direction of incident positron beams in the target chamber. The SDD detector, which was used to record the x rays emitted from the target impacted by the positron, was right over the target along the Z axis in the chamber. A high-purity germanium detector (HPGe) [23], which was applied to record the annihilation γ rays emitted from the target bombarded by the positron, was outside of the target chamber. Its center axis was along the Y-coordinate axis.

The SDD detector used in this work has an excellent detection performance for low-energy x rays; it has an energy resolution [full width at half maximum (FWHM)] of 139 eV

at ^{55}Fe 5.9-keV K_α x ray. Its active area is 80 mm^2, and the thickness of the detector's sensitive layer is only 0.45 mm (adopting a large probe can make SDD more efficient in collecting interesting characteristic x-ray counts; adopting the very thin sensitive layer can reduce the backgrounds resulting from the annihilation γ rays). The efficiency calibration of the SDD detector in the low-energy region was performed as follows [24]: The experimental bremsstrahlung spectra by 19-keV electrons bombarding high-purity thick carbon were collected by the SDD detector, and the theoretical bremsstrahlung spectra were acquired with the PENELOPE-2005 code [25] by simulating 19-keV electrons impacting on the thick carbon target. The relative efficiency calibration curve was determined from the ratio of the experimental bremsstrahlung spectra to the theoretical bremsstrahlung spectra, and the absolute efficiency calibration curve of the SDD detector was obtained by the detection efficiency of ^{241}Am radioactive standard point source at the 13.9-keV energy peak [24].

The incident positron number $N_{e+}(E_0)$ was obtained by an online monitoring technology based on the formula proposed by our group in Ref. [26]:

$$N_{e+}(E_0) = \frac{N_\gamma(E_0)}{\xi(E_0)\varepsilon_{\mathrm{EXP}}/\varepsilon_{\mathrm{MC}}}. \tag{1}$$

Here $N_\gamma(E_0)$ denotes the counts of 511-keV γ photons recorded by the HPGe detector when positrons with the incident energy E_0 bombard the thick target in the experiment. $\xi(E_0)$ is the average number of 511-keV γ photons collected by the HPGe detector when a positron with incident energy E_0 impacts on the thick target; it is obtained with a Monte Carlo code [25] by simulating the real experiment. $\varepsilon_{\mathrm{EXP}}$ is the absolute detection efficiency of the HPGe detector at the 511-keV γ energy peak; it was measured by using standard point sources placed at the target position. $\varepsilon_{\mathrm{MC}}$ is similar to $\varepsilon_{\mathrm{EXP}}$ but calculated by Monte Carlo simulation [25].

The typical characteristic x-ray spectra for Pb and Bi targets impacted by 8-keV positrons are displayed in Figs. 2(a) and 2(b), respectively.
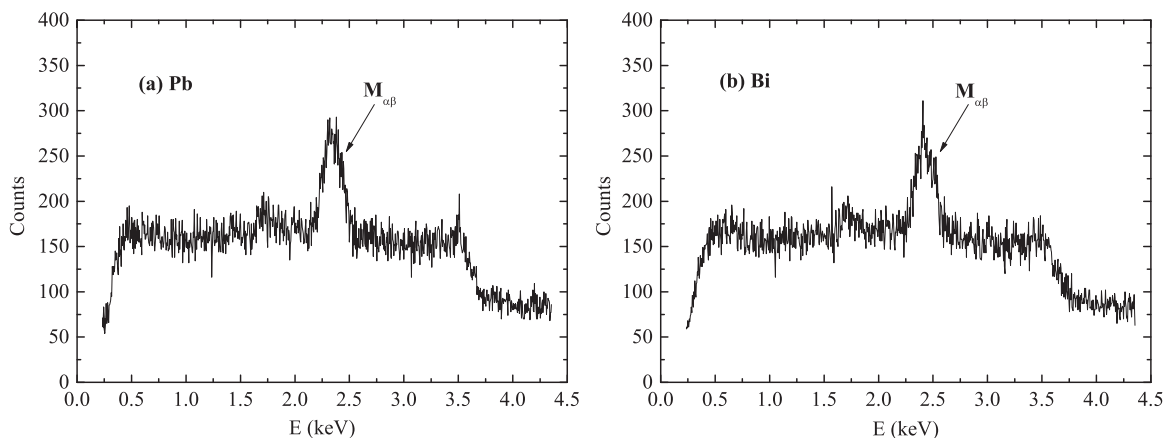

FIG. 2. Typical characteristic x-ray spectra for Pb and Bi targets impacted by 8-keV positrons.

B. Data processing

If the effects of the multiple scattering of incident positrons in the thick target, from the bremsstrahlung photons and annihilation photons and the other secondary particles on the characteristic x rays are disregarded [19], the characteristic x-ray yield Y_{e+} for atomic inner-shell ionization induced by incident positron is indicated as in Eq. (2) [19]:

$$Y_{e+}(E_0) = \frac{N_A}{A} \varepsilon \int_I^{E_0} \sigma_{\mathrm{x}}(E) e^{-\mu_{\mathrm{x}} \frac{\cos\alpha}{\cos\beta} \int_E^{E_0} \frac{dE^*}{S(E^*)}} \frac{dE}{S(E)},$$
(2)

where E_0 represents the incident positron energy, I is the atomic ionization threshold energy, N_A is the Avogadro constant, A is the atomic mass number, ε is the SDD detector's absolute detection efficiency at the atomic characteristic x-ray energy, σ_{x} is the characteristic x-ray production cross section, μ_{x} is the mass attenuation coefficient for the characteristic x-ray inside the target, $S(E)$ is the mass stopping power, α is the angle between the incident direction and the target normal, and β is the angle between the x-ray detector direction and the target normal.

In fact, in the incident energy region of this work, the multiple scattering of incident positrons in the thick target should be considerable, the photons can cause photoionization, and other secondary particles can induce atomic inner-shell ionization. These effects can contribute to the characteristic x-ray yield. If the contribution share of these factors to characteristic x-ray yield is defined as the correction factor f,

Eq. (2) should be modified as in Eq. (3) [27]:

$$[1 - f(E_0)]Y(E_0)$$
$$= Y_{e+}(E_0) = \frac{N_A}{A} \varepsilon \int_I^{E_0} \sigma_{\mathrm{x}}(E) e^{-\mu_{\mathrm{x}} \frac{\cos\alpha}{\cos\beta} \int_E^{E_0} \frac{dE^*}{S(E^*)}} \frac{dE}{S(E)}, \quad (3)$$

where Y is the characteristic x-ray yields induced by all kinds of particles in the experiment, and the definitions of other symbols are the same as in Eq. (2). The correction factor $f(E_0)$ can be obtained by the following method:

$$f(E_0) = \frac{Y_{\mathrm{MC}}(E_0) - Y'_{e+}(E_0)}{Y_{\mathrm{MC}}(E_0)}. \quad (4)$$

Here $Y_{\mathrm{MC}}(E_0)$ is the total characteristic x-ray yields calculated with PENELOPE-2005 code [25]; it is acquired by realistically simulating the experiment of positrons with incident energy E_0 bombarding the thick target. $Y'_{e+}(E_0)$ is one part of $Y_{\mathrm{MC}}(E_0)$, and it is the characteristic x-ray yields induced directly by positrons whose scattering effect in the thick target is ignored. $Y'_{e+}(E_0)$ can be calculated by integration according to Eq. (5).

$$Y'_{e+}(E_0) = \frac{N_A}{A} \frac{\Omega}{4\pi} \int_I^{E_0} \sigma_{\mathrm{x},th}(E) e^{-\mu_{\mathrm{x}} \frac{\cos\alpha}{\cos\beta} \int_E^{E_0} \frac{dE^*}{S(E^*)}} \frac{dE}{S(E)}. \quad (5)$$

Here Ω is the solid angle of the SDD detector at the collision point in our experiment. $\sigma_{\mathrm{x},th}$ is the theoretical characteristic x-ray production cross sections; it can be calculated from the inner-shell ionization cross sections and the atomic relaxation parameters. The definitions of other symbols are the same as in Eq. (2).

The M_α and M_β x-ray production cross sections used in this work can be calculated according to Eqs. (6) and (7) [28].

$$\sigma_{M\alpha} = \frac{\Gamma_{M_5 N_{6,7}}}{\Gamma_{M_5 \text{Total}}} \omega_{M_5} \Big\{ \sigma_{M_5} + \sigma_{L_1} n_{L_1 M_5} + \sigma_{L_2} n_{L_2 M_5} + \sigma_{L_3} n_{L_3 M_5} + \big(\sigma_{M_4} + \sigma_{L_1} n_{L_1 M_4} + \sigma_{L_2} n_{L_2 M_4} + \sigma_{L_3} n_{L_3 M_4} \big) f_{45}$$
$$+ \big(\sigma_{M_3} + \sigma_{L_1} n_{L_1 M_3} + \sigma_{L_2} n_{L_2 M_3} + \sigma_{L_3} n_{L_3 M_3} \big)(S_{35} + S_{34} f_{45}) + \big(\sigma_{M_2} + \sigma_{L_1} n_{L_1 M_2} + \sigma_{L_2} n_{L_2 M_2} + \sigma_{L_3} n_{L_3 M_2} \big)$$
$$\times [S_{25} + S_{23} S_{35} + f_{45}(S_{24} + S_{23} S_{34})] + \big(\sigma_{M_1} + \sigma_{L_1} n_{L_1 M_1} + \sigma_{L_2} n_{L_2 M_1} + \sigma_{L_3} n_{L_3 M_1} \big)[S_{15} + S_{12} S_{25} + S_{13} S_{35}$$
$$+ S_{12} S_{23} S_{35} + f_{45}(S_{14} + S_{12} S_{24} + S_{13} S_{34} + S_{12} S_{23} S_{34})] \Big\},$$
(6)

$$\sigma_{M\beta} = \frac{\Gamma_{M_4 N_6}}{\Gamma_{M_4 \text{Total}}} \omega_{M_4} \Big\{ \sigma_{M_4} + \sigma_{L_1} n_{L_1 M_4} + \sigma_{L_2} n_{L_2 M_4} + \sigma_{L_3} n_{L_3 M_4} + \big(\sigma_{M_3} + \sigma_{L_1} n_{L_1 M_3} + \sigma_{L_2} n_{L_2 M_3} + \sigma_{L_3} n_{L_3 M_3} \big) S_{34}$$
$$+ \big(\sigma_{M_2} + \sigma_{L_1} n_{L_1 M_2} + \sigma_{L_2} n_{L_2 M_2} + \sigma_{L_3} n_{L_3 M_2} \big)(S_{23} S_{34} + S_{24}) + \big(\sigma_{M_1} + \sigma_{L_1} n_{L_1 M_1} + \sigma_{L_2} n_{L_2 M_1} + \sigma_{L_3} n_{L_3 M_1} \big)$$
$$\times (S_{12} S_{23} S_{34} + S_{13} S_{34} + S_{12} S_{24} + S_{14}) \Big\}.$$
(7)

In Eqs. (6) and (7), σ_{Li} and σ_{Mi} are the L-subshell and M-subshell ionization cross sections, respectively; the other symbols are the atomic parameters whose definitions were listed in Ref. [28].

When calculating the correction factor $f(E_0)$, the inner-shell ionization cross sections and the atomic relaxation parameters used to calculate the $\sigma_{\mathrm{x},th}$ in Eq. (5) are all taken from the database of PENELOPE-2005 [25]; i.e., the data of inner-shell ionization cross sections by lepton impact are taken from the DWBA model, and the data of atomic relaxation are extracted from the LLNL Evaluated Atomic Data Library (EADL [29]). Additionally, the mass attenuation coefficient for the characteristic x-ray inside the target and the mass

stopping power in Eq. (5) are also extracted from the database of PENELOPE-2005 [25].

$f(E_0)$ calculated in this work is plotted in Fig. 3. As can be seen, in the incident energy region of this work, the influence of the multiple scattering of incident positrons, from the bremsstrahlung and annihilation photons and other secondary particles on the characteristic x-ray yields, cannot be ignored, and $f(E_0)$ is bigger as the incident positron energy is nearer the ionization threshold energy.

Then the algorithm of converting the experimental characteristic x-ray yield to the corresponding characteristic x-ray production cross sections according to Eq. (3) needs to be studied. Equation (3) is a Fredholm integral equation of the first
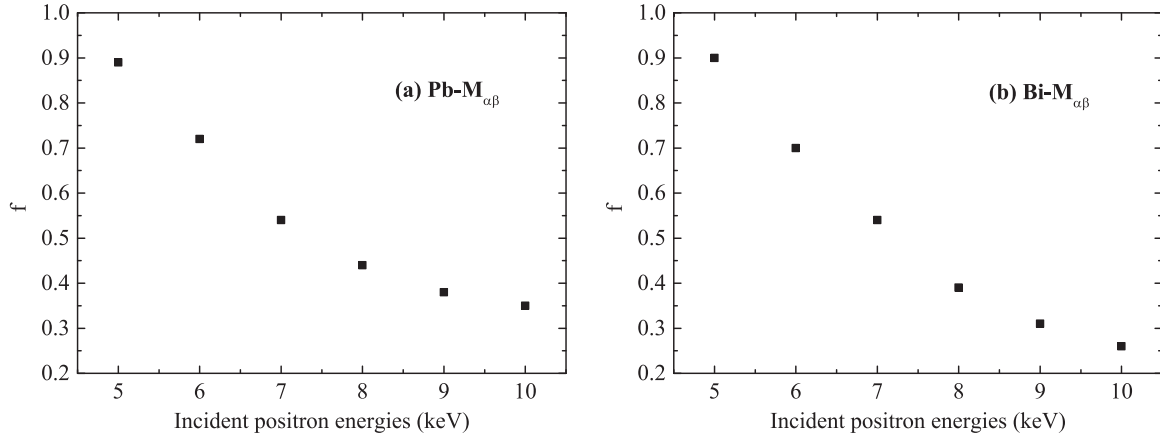
FIG. 3. Correction factor $f(E_0)$ for $M_{\alpha\beta}$ characteristic x-ray yields of Pb and Bi.

kind and its solution is typically an ill-posed problem [19]. An *et al.* [19] have adopted the Tikhonov regularization method to solve the problem about K-shell ionization cross sections. If experimental characteristic x-ray energy peaks of a certain inner shell cannot be divided into their respective subpeaks, such as M_{α} and M_{β} of Pb or Bi in this measurement, Eq. (3) is invalid because μ_x are not the same for x rays at different energies. Of course, it is not a problem for the K shell, because there are only two characteristic x-ray subpeaks for K lines; i.e., K_{α} and K_{β}. $K_{\alpha\beta}$ x-ray production cross sections can be separated into K_{α} and K_{β} by K_{α} x-ray emission rate. Based on this, Zhu *et al.* [20] have obtained the $K_{\alpha\beta}$ x-ray production cross sections of Si by using the Tikhonov regularization method. However, there are more subpeaks for L or M lines; characteristic x-ray production cross sections of these subpeaks cannot be acquired by x-ray emission rates simply.

Here the theoretical M_{α} and M_{β} x-ray yields for Pb and Bi were calculated according to Eq. (5), in which the theoretical x-ray production cross sections are acquired by the DWBA [3,6] or PWBA [5] models combined with the atomic relaxation parameters reported by Puri *et al.* [30–32]. Then, the theoretical ratios of the M_{α} characteristic x-ray yields $Y(M_{\alpha})$ to $M_{\alpha\beta}$ yields $Y(M_{\alpha\beta})$ for Pb and Bi were obtained and displayed in Fig. 4. Thus, our measured $M_{\alpha\beta}$ characteristic x-ray yields of

Pb and Bi could be separated into M_{α} and M_{β} yields by the theoretical ratios $Y(M_{\alpha})/Y(M_{\alpha\beta})$ obtained from DWBA-Puri or PWBA-Puri. And then, with the Tikhonov regularization method, the experimental M_{α} and M_{β} x-ray production cross sections of Pb and Bi could be solved by the corresponding characteristic x-ray yield, and they are depicted in Fig. 5. Finally, the experimental $M_{\alpha\beta}$ x-ray production cross sections of Pb and Bi are the sum of the experimental M_{α} and M_{β} x-ray production cross sections.

III. RESULTS AND DISCUSSION

Our experimental data of the $M_{\alpha\beta}$ x-ray production cross sections for Pb and Bi elements are shown in Figs. 6 and 7, respectively. The experimental uncertainties mainly come from the characteristic x-ray peak net counts ($\sim$2% for Pb and Bi), the background subtraction ($\sim$1%), the SDD's detection efficiency at the low-energy region ($\sim$8%), the incident positrons number ($\sim$5%), the mass attenuation coefficient ($\sim$5%) and the mass stopping power ($\sim$5%) [19], the Tikhonov regularization method ($\sim$5%) [19], and the Monte Carlo simulation in the calculation of the correction factor f ($\sim$2% for Pb and $\sim$3% for Bi). Therefore, the global uncertainties are $\sim$13% for both Pb and Bi elements.
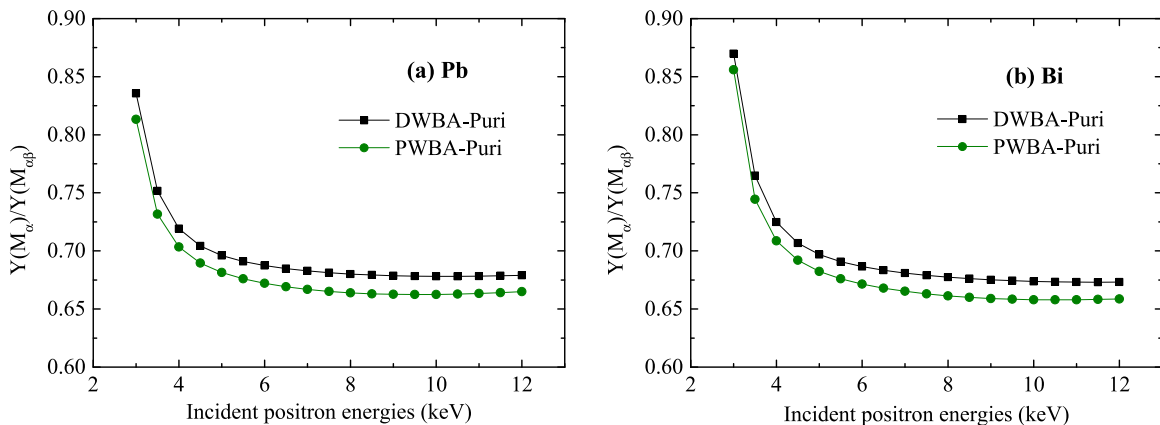

FIG. 4. Ratios of the M_{α} characteristic x-ray yields to $M_{\alpha\beta}$ yields calculated by DWBA-Puri theoretical predictions ■ and PWBA-Puri theoretical predictions ●, respectively.

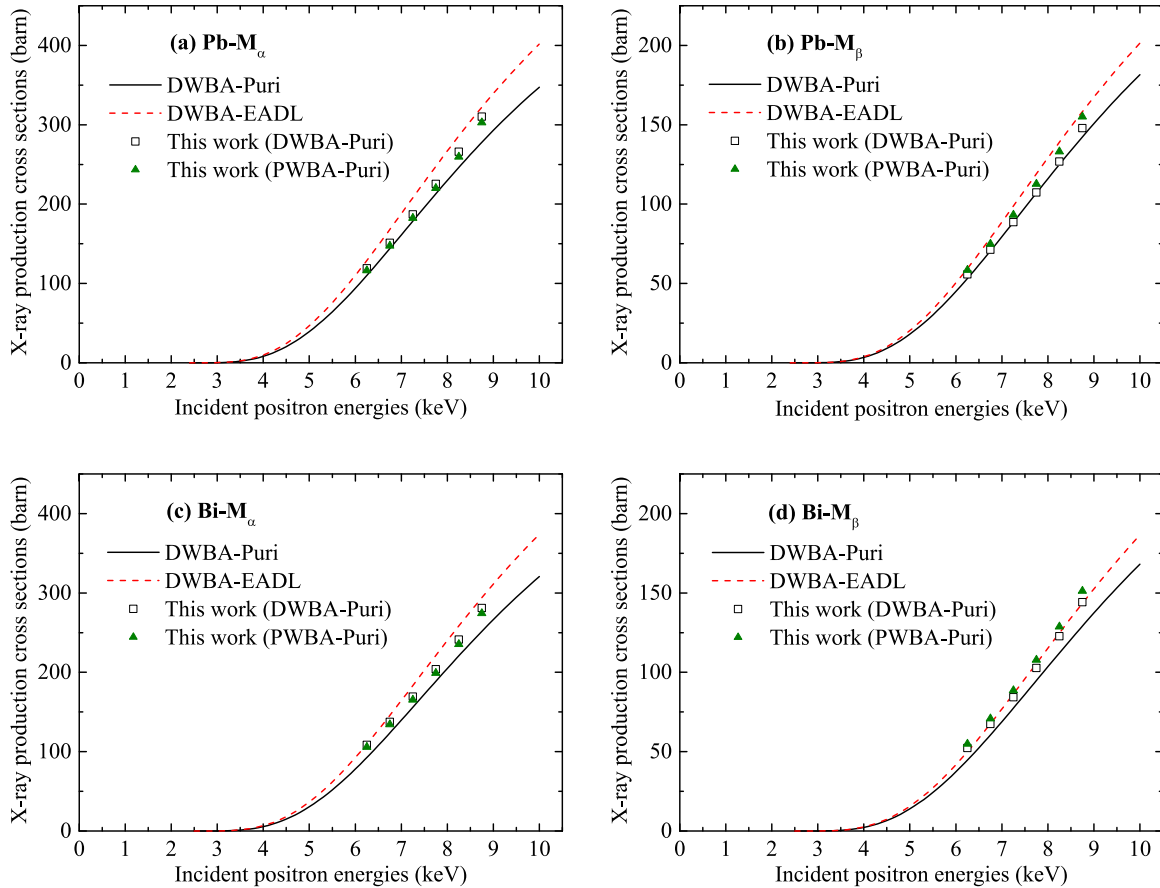FIG. 5. M_α and M_β x-ray production cross sections for Pb and Bi calculated by the Tikhonov regularization method [□ represents the results based on $Y(M_\alpha)/Y(M_{\alpha\beta})$ calculated with DWBA-Puri; ▲ represents the results based on $Y(M_\alpha)/Y(M_{\alpha\beta})$ calculated with PWBA-Puri]. The DWBA theoretical predictions are also presented.
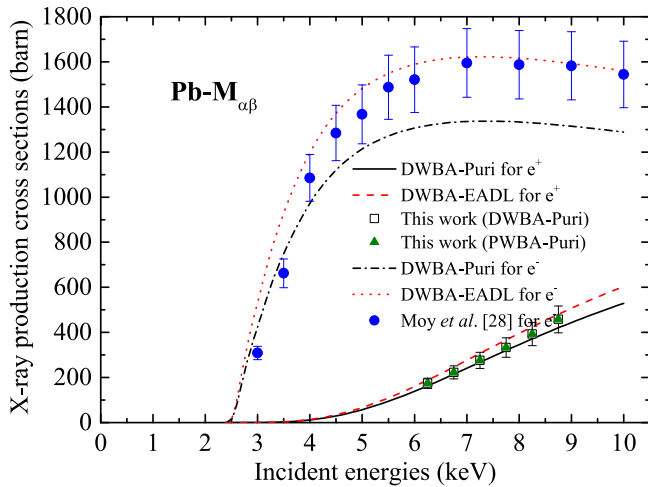

FIG. 6. $M_{\alpha\beta}$ x-ray production cross sections for Pb impacted by positrons calculated by the Tikhonov regularization method [□ represents the results based on $Y(M_\alpha)/Y(M_{\alpha\beta})$ obtained with DWBA-Puri; ▲ represents the results based on $Y(M_\alpha)/Y(M_{\alpha\beta})$ obtained with PWBA-Puri] in comparison with the DWBA theoretical predictions. The experimental data for electron impact published by Moy *et al.* [28] (●) and the corresponding DWBA theoretical predictions are also presented.
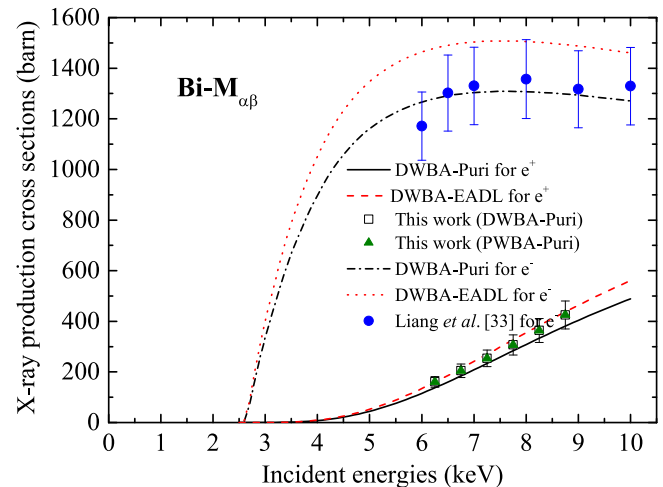

FIG. 7. $M_{\alpha\beta}$ x-ray production cross sections for Bi impacted by positrons calculated by the Tikhonov regularization method [□ represents the results based on $Y(M_\alpha)/Y(M_{\alpha\beta})$ obtained with DWBA-Puri; ▲ represents the results based on $Y(M_\alpha)/Y(M_{\alpha\beta})$ obtained with PWBA-Puri] in comparison with the DWBA theoretical predictions. The experimental data for electron impact in our previous work [33] by using the thin film deposited on self-supporting thin C film (●) and the corresponding DWBA theoretical predictions are also presented.

TABLE I. $M_{\alpha\beta}$ x-ray production cross sections for Pb and Bi elements calculated by the Tikhonov regularization method.

E (keV)	$M_{\alpha\beta}$ x-ray production cross sections (barns)	
	Pb	Bi
6.25	175	161
6.75	222	205
7.25	276	254
7.75	333	307
8.25	393	364
8.75	458	425

As shown in Figs. 4(a) and 4(b), there is a small gap (<3% for Pb and Bi) between the theoretical ratios $Y(M_\alpha)/Y(M_{\alpha\beta})$ calculated from DWBA-Puri and PWBA-Puri; hence, whether for the M_α line or the M_β line, the experimental x-ray production cross sections based on these two ratios have a slight difference. After the sum of experimental M_α and M_β x-ray production cross sections, nevertheless, as illustrated in Figs. 6 and 7, the experimental $M_{\alpha\beta}$ x-ray production cross sections based on the ratios $Y(M_\alpha)/Y(M_{\alpha\beta})$ calculated from DWBA-Puri and PWBA-Puri are nearly identical (the deviations are <0.1% for Pb and Bi). These results show that experimental $M_{\alpha\beta}$ x-ray production cross sections acquired in this work are independent from the theoretical models used in the calculation of the ratios $Y(M_\alpha)/Y(M_{\alpha\beta})$. Table I lists the experimental data of $M_{\alpha\beta}$ x-ray production cross sections for Pb and Bi, which are the average of $M_{\alpha\beta}$ x-ray production cross sections based on the ratios $Y(M_\alpha)/Y(M_{\alpha\beta})$ obtained with DWBA-Puri and PWBA-Puri. According to the error transfer formula, the errors of the experimental data in Table I are all ~12%.

In Figs. 6 and 7, our experimental data of $M_{\alpha\beta}$ x-ray production cross sections for Pb and Bi are, respectively, compared with the corresponding DWBA theoretical values, which are acquired by the DWBA model combined with two different sets of atomic relaxation parameters reported, respectively, by

Puri *et al.* [30–32] and EADL [29]. Moreover, the experimental data of Pb $M_{\alpha\beta}$ induced by electron which were reported by Moy *et al.* [28] (by M_α x-ray production cross sections plus M_β cross sections of Moy *et al.* [28]) and the corresponding DWBA theoretical values are also plotted in Fig. 6, and the experimental data of Bi $M_{\alpha\beta}$ induced by electrons in our previous work [33] and the corresponding DWBA theoretical values are also displayed in Fig. 7. For positron impact, Figs. 6 and 7 show that the difference between DWBA-Puri theoretical values and DWBA-EADL theoretical values is about 16% for Pb and about 17% for Bi, and the DWBA theoretical values are in good agreement with the present experimental data of both Pb and Bi. For electron impact, the gap between DWBA-Puri theoretical values and DWBA-EADL theoretical values is ~22% for Pb and ~16% for Bi. In Fig. 6, for Pb impacted by electrons up to 10 keV, DWBA-EADL predictions give a good description of the experimental data reported by Moy *et al.* [28], while DWBA-Puri predictions underestimate the experimental data by ~17%; in Fig. 7, for Bi impacted by electrons up to 10 keV, DWBA-Puri predictions are in good accordance with the experimental data in our previous work [33], while DWBA-EADL predictions overestimate the experimental data by ~12%. Therefore different selection of the atomic parameters used in the calculation of the theoretical M-shell x-ray production cross sections has some influence on the degree of difference between the DWBA theoretical predictions and the experimental data, and it is more pronounced for electron impact.

In Fig. 8, we also compared the ratios of the $M_{\alpha\beta}$ x-ray production cross sections for Pb and Bi impacted by electrons to those by positrons. The experimental data for positron impact are originated from Table I, and the experimental data for electron impact are extracted from Refs. [28,33] (to acquire the experimental data for electron impact with the same incident energies as those by positron impact, the experimental data for electron impact in Refs. [28,33] were interpolated at some certain incident energies). The uncertainties of experimental ratios can be obtained by the error transfer formula.

As observed from Fig. 8, the ratios $\sigma(e^-)/\sigma(e^+)$ calculated by DWBA predictions based on two different atomic relaxation
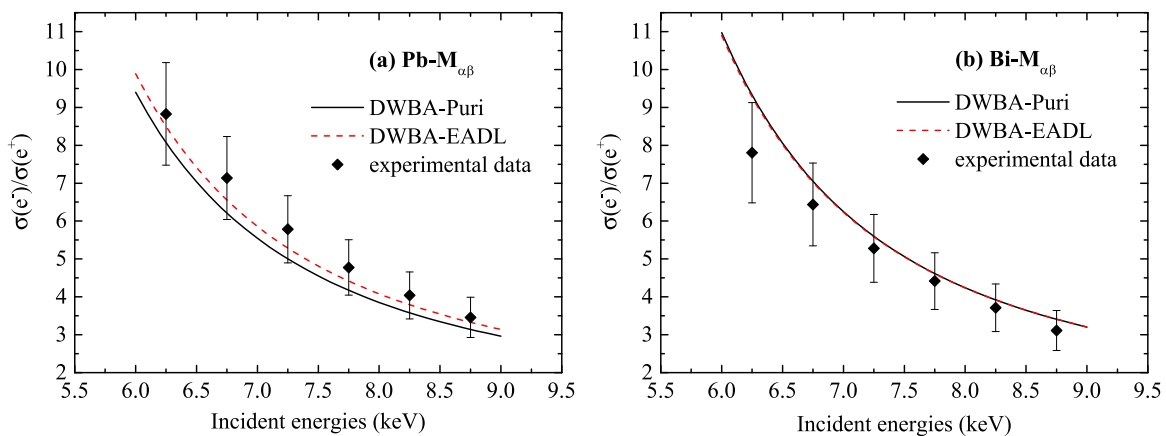

FIG. 8. Ratios of the $M_{\alpha\beta}$ x-ray production cross sections by electron impact to that by positron impact. ◆ represents the ratios of the experimental data by electron impact published in Ref. [28] or Ref. [33] to that by positron impact in this work. The solid line and the dashed line represent the ratios $\sigma(e^-)/\sigma(e^+)$ calculated by DWBA-Puri and DWBA-EADL theoretical predictions, respectively.

parameters are very close (the deviations are <0.1% for Pb and Bi). The influence of different selection of the atomic relaxation parameters on the DWBA theoretical ratios $\sigma(e^-)/\sigma(e^+)$ is much smaller than that of the $M_{\alpha\beta}$ x-ray production cross sections predicted by the DWBA model. The DWBA theoretical ratios $\sigma(e^-)/\sigma(e^+)$ are in good accordance with the experimental ratios $\sigma(e^-)/\sigma(e^+)$ within the experimental errors; this shows that DWBA could give a good description of the M-shell ionization process for Pb and Bi impacted by both electrons and positrons near the threshold energy. As mentioned in the first section, the experimental data for positron impact near the ionization threshold energy are still scarce; to give a full check to the advanced theoretical models recently developed, more reliable measurements for positron impact need to be done in the future.

IV. CONCLUSIONS

The $M_{\alpha\beta}$ x-ray production cross sections for Pb and Bi impacted by 6–9-keV positrons have been measured by using the thick-target method. In the experiment, we applied an online monitoring technology to obtain an accurate number of incident positrons bombarding the thick targets, and adopted a Monte Carlo simulation in combination with theoretical integral calculation to eliminate the influences of the multiple scattering of incident positrons, from the bremsstrahlung and annihilation photons and other secondary particles on the characteristic x-ray yields. The Tikhonov regularization method was used to acquire the $M_{\alpha\beta}$ x-ray production cross sections of Pb and Bi by positron impact. Our results were compared with the DWBA theoretical predictions, which shows that the DWBA theory could provide a good description for the M-shell ionization process for Pb and Bi impacted by positrons near the threshold energy.

[1] C. J. Powell, in *Electron Impact Ionization*, edited by T. D. Mark and G. H. Dunn (Springer-Verlag, New York, 1985), Chap. 6.

[2] R. Hippler, Phys. Lett. A **144**, 81 (1990).

[3] S. Segui, M. Dingfelder, and F. Salvat, Phys. Rev. A **67**, 062710 (2003).

[4] S. Luo and D. C. Joy, in *Microbeam Analysis*, edited by D. G. Howitt (San Francisco Press, San Francisco, 1991), pp. 67–68.

[5] S. P. Khare and J. M. Wadehra, Can. J. Phys. **74**, 376 (1996).

[6] J. Colgan, C. J. Fontes, and H. L. Zhang, Phys. Rev. A **73**, 062711 (2006).

[7] X. Llovet, C. J. Powell, F. Salvat, and A. Jablonski, J. Phys. Chem. Ref. Data **43**, 013102 (2014).

[8] C. Merlet, A. Moy, X. Llovet, and O. Dugne, Surf. Interface Anal. **46**, 1170 (2014).

[9] A. Sepúlveda, A. P. Bertol, M. A. Z. Vasconcellos, J. Trincavelli, R. Hinrichs, and G. Castellano, J. Phys. B: At., Mol. Opt. Phys. **47**, 215006 (2014).

[10] J. L. Zhao, Z. An, J. J. Zhu, W. J. Tan, and M. T. Liu, Radiat. Phys. Chem. **122**, 66 (2016).

[11] J. L. Zhao, Z. An, J. J. Zhu, W. J. Tan, and M. T. Liu, Radiat. Phys. Chem. **134**, 71 (2017).

[12] C. S. Mei, Y. Wu, Y. Yuan, C. H. Chang, Z. C. Qian, J. J. Zhu, and K. Moharram, J. Phys. B: At., Mol. Opt. Phys. **49**, 245204 (2016).

[13] Z. C. Qian, Y. Wu, C. H. Chang, Y. Yuan, C. S. Mei, J. J. Zhu, and K. Moharram, Europhys. Lett. **118**, 13001 (2017).

[14] Y. Nagashima, F. Saito, Y. Itoh, A. Goto, and T. Hyodo, Phys. Rev. Lett. **92**, 223201 (2004).

[15] Y. Nagashima, W. Shigeta, T. Hyodo, and M. Iwaki, Radiat. Phys. Chem. **76**, 465 (2007).

[16] T. Mukoyama, Y. Nagashima, and K. Tokési, Nucl. Instrum. Methods Phys. Res., Sect. B **279**, 41 (2011).

[17] L. X. Tian, M. T. Liu, J. J. Zhu, Z. An, B. Y. Wang, and X. B. Qin, Plasma Sci. Technol. **14**, 434 (2012).

[18] VITUS H80 type, Ketek Corporation.

[19] Z. An and Q. Hou, Phys. Rev. A **77**, 042702 (2008).

[20] J. J. Zhu, Z. An, M. T. Liu, and L. X. Tian, Phys. Rev. A **79**, 052710 (2009).

[21] C. Q. He, J. C. Wang, J. Zhu, and S. J. Wang, Mater. Sci. Forum **733**, 314 (2013).

[22] P. Kuang, X. L. Han, X. Z. Cao, R. Xia, P. Zhang, and B. Y. Wang, Chin. Phys. B **26**, 057802 (2017).

[23] GEM20P4 type, ORTEC Corporation.

[24] C. H. Chang and Y. Wu, in *Progress Report on China Nuclear Science & Technology*, edited by Z. Fu (China Atomic Energy Press, Beijing, 2017), Vol. 9, pp. 74–79 (in Chinese).

[25] F. Salvat, J. M. Fernández-Varea, and J. Sempau, PENELOPE-2005, A code system for Monte Carlo simulation of electron and photon transport, OECD/NEA Data.

[26] Y. Yuan and Y. Wu, in *Progress Report on China Nuclear Science & Technology*, edited by Z. Fu (China Atomic Energy Press, Beijing, 2017), Vol. 9, pp. 68–73 (in Chinese).

[27] L. X. Tian, Ph.D. thesis, Sichuan University, 2010 (in Chinese).

[28] A. Moy, C. Merlet, X. Llovet, and O. Dugne, J. Phys. B: At., Mol. Opt. Phys. **46**, 115202 (2013).

[29] S. T. Perkins, D. E. Cullen, M. H. Chen, J. H. Hubbell, J. Rath, and J. Scofield, Report UCRL-50400, Vol. 30, Lawrence Livermore National Laboratory, Livermore, CA, 1991.

[30] Y. Chauhan and S. Puri, At. Data Nucl. Data Tables **94**, 38 (2008).

[31] Y. Chauhan, A. Kumar, and S. Puri, At. Data Nucl. Data Tables **95**, 475 (2009).

[32] S. Puri, At. Data Nucl. Data Tables **93**, 730 (2007).

[33] Y. Liang, M. X. Xu, Y. Yuan, Y. Wu, Z. C. Qian, C. H. Chang, C. S. Mei, J. J. Zhu, and K. Moharram, Radiat. Phys. Chem. **141**, 17 (2017).